Conformational Study of Eugenol by Density Functional Theory Method and Matrix-Isolation Infrared Spectroscopy

Adriana Olbert-Majkut and Maria Wierzejewska*

Faculty of Chemistry, Wrocław University, F.Joliot-Curie 14, 50-383 Wrocław, POLAND

Received: February 18, 2008; Revised Manuscript Received: April 15, 2008

The B3LYP/6-311++G(2d,2p) study of the potential energy surface of eugenol (4-allyl-2-methoxyphenol, 2-methoxy-4-pro-2-emyl-phenol) was performed with the aim of finding all possible conformers of the molecule. Twelve conformers were found belonging to one of three groups differing in the relative orientation of the OH and OCH_3 moieties: SA (syn-anti), AA (antianti) and AG (antigauche). The lowest-energy conformers of eugenol (SAA+, SAA− and SAS) stabilized by the intramolecular hydrogen bond differ only in the arrangement of the allyl group with respect to the aromatic ring. The calculated abundance of all three SA species equals 99.8% whereas the remaining AA and AG show the negligible population of 0.2%. In consonance with theoretical predictions, only syn-anti conformers are present in the low temperature matrices studied. The presented FTIR results allow, for the first time, unequivocal identification and spectral characterization of three SA conformers of the eugenol molecule isolated in solid argon and xenon. The performed studies reveal that conformational cooling (upon increasing the substrate temperature during deposition) takes place in the studied matrices and that the less stable SAA− and SAS species convert into SAA+. This observation appears to be consistent with the theoretically predicted energy barriers of 6.70 and 10.45 kJ/mol for the SAA− → SAA+ and SAS → SAA+ interconversions which are low enough to be surpassed during deposition at higher temperatures.

I. Introduction

Eugenol, the major phenolic component of clove oil is widely used in medical and dental practices. In the last decades many studies have been performed on its interesting and useful attributes.[1–6] Eugenol possesses analgesic, anti-inflammatory and anesthetic properties. It also exhibits antimicrobial-, and anti-aggregating activity as is reflected by its influence on platelet function studied ex vivo.[7] Recently, it was shown that eugenol is an active antifungal agent with potential therapeutic implications for Biofilm-associated candidal infections.[8] In addition, eugenol shows potential antitumor properties thanks to the presence of the phenolic group which produces radical-scavenging activity. Some of these attributes are associated with the coexistance of hydrophilic and hydrophobic moieties within the molecule.

Understanding the conformational behavior of eugenol is expected to provide useful insights into the source of its biological function. In spite of the widespread applications of eugenol, only a few papers devoted to this topic have been published. Moreover, no reports on the detailed conformational analysis or rotational isomerization processes of the eugenol molecule are available in the literature. Castaño and co-workers have studied eugenol, eugenol−$(H_2O)_n$ complexes[9] and eugenol dimers[10] in a supersonic expansion using a number of laser spectroscopic mass-resolved techniques. The authors also reported the results of theoretical calculations at different levels of theory for the studied species. For the eugenol monomer, three conformers were considered characterized by the intramolecular hydrogen bond between the OH and OCH_3 groups. Two of these conformers were identified in the experimental spectra, and it was concluded that the low energy barrier between two of the conformers allows for the changes of the population of the species at the supersonic conditions.[9]

The matrix isolation technique in combination with FTIR spectroscopy proved to be a powerful tool for conformational studies.[11] It has been directly demonstrated for many systems that the high temperature concentration ratio may be preserved in low temperature matrices due to the fast cooling of the gaseous mixture of the isomers. This is often the case when the barriers for intramolecular rearrangements are higher than ca. 10−11 kJ/mol.[12] However, it might be that the abundance of the conformers in low temperature matrices does not correspond to the gas phase population. The gas phase abundance may change because of the conformer interconversion during its deposition. The degree of this process, called conformational cooling, depends on several factors, such as nature of the matrix and matrix-isolated guest, relative energies of conformers and energy barriers, dipole moments of the conformers and temperature of the substrate during deposition.[13] In addition, upon annealing of the deposited matrix, the provided thermal energy can be sufficient to overcome some barriers allowing the system to evolve into the equilibrium at the matrix temperature. Conformational cooling is expected to occur in matrices for various compounds characterized by low energy barriers to internal rotation. A number of examples of this process occurring in low temperature matrices for various molecules has been reported in the literature: cyanoacetic acid,[13] glycine,[14] 1,2-dichloroethane,[15] 1,2-butanediol,[16] glycolic acid,[17] trimethyl phosphate[18] and dimethyl sulfite.[19]

The eugenol molecule in low temperature matrices has not yet been studied. Here, conformational analysis of this compound isolated in argon and xenon was performed by means of matrix isolation and FTIR spectroscopy allowing for vibrational characterization of the most stable conformers. The experimental

* To whom correspondence should be addressed: Fax: +48-71-328-2348. E-mail: mariaw@wchuwr.pl.

10.1021/jp801430d CCC: $40.75
Published on Web 06/04/2008

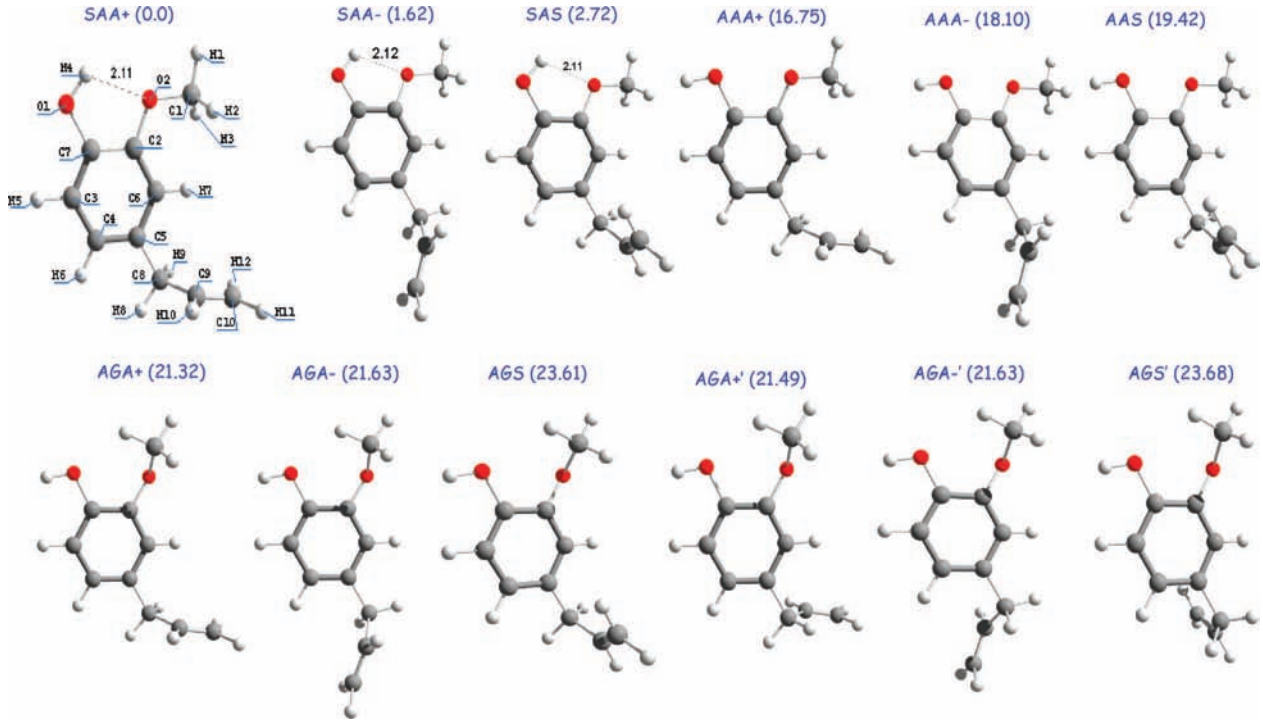

Figure 1. B3LYP/6-311++G(2d,2p) optimized geometries of the eugenol conformers. The values of the zero-point-corrected energy relative to the most stable conformer (kJ/mol) are given in parentheses.

results are supported by theoretical calculations. A systematic search for the possible minima on the potential energy surface (PES) of the monomeric eugenol molecule was carried out at the B3LYP/6-311++G(2d,2p) level of theory.

II. Experimental Section

II.1. Computational Details. All calculations were performed with the Gaussian 03 program package.[20] Structures of the minima were optimized at the B3LYP/6-311++G(2d,2p) level. The associated force constant matrixes were calculated to evaluate harmonic frequencies and zero-point vibrational (ZPE) corrections. The calculated frequencies were scaled by 0.944 above 2000 cm^{-1} and by 0.979 for the 2000−500 cm^{-1} spectral region. The scaling factors were determined by linear fitting with intercept zero. For the fingerprint region eighteen experimental and calculated frequencies of the SAA+ conformer were used. Three transition states linking the SA conformers were localized on the PES and verified by the presence of one imaginary vibrational frequency. The corresponding SA minima were connected to each TS by following intrinsic reaction coordinate (IRC) generated at the B3LYP/6-311++G(2d,2p) level. All energies discussed throughout the paper are those with the zero point vibrational energy correction included.

II.2. Infrared Spectroscopy. Eugenol was evaporated from a small glass bulb containing a liquid sample held at room temperature. The container was placed outside the vacuum vessel of the cryostat and the eugenol vapor was mixed with a matrix gas (Ar or Xe) at ca. 5 cm distance from the cold substrate. An accurate concentration of the sample in matrices was not known, but it could be varied by changing the pressure of the matrix gas deposited. Most spectra were taken at such conditions that allowed us to avoid eugenol aggregation. The gas mixtures were condensed onto a gold-plated copper mirror maintained at a low temperature by means of a closed cycle helium refrigerator (Air Products, Displex 202A). Different substrate temperatures during deposition were used: 11−30 K (Ar) and 20−50 K (Xe). After deposition of the matrices, subsequent annealing experiments were performed. Infrared spectra were recorded between 4000−500 cm^{-1} in a reflection mode with a resolution of 0.5 cm^{-1} by means of a Bruker 113v FTIR spectrometer equipped with liquid N_2 cooled MCT detector.

III. Results and Discussion

III.1. Geometries and Energetics. The eugenol molecule has four internal rotation axes that give rise to a number of different conformational isomers. A systematic search on the PES of the eugenol molecule revealed the presence of twelve conformers, all belonging to the C_1 symmetry point group. The optimized geometries of these conformers calculated at the B3LYP/6-311++G(2d,2p) level are shown in Figure 1 together with the adopted numbering scheme. The key torsional angles, relative energies, relative Gibbs free energies and abundances at 298 K for all these species are gathered in Table 1. Each of the twelve conformers has its mirror-image structure of the same energy; these species will not be considered further.

All studied conformers belong to one of three groups differing in the relative orientation of the OH and OCH_3 moieties: SA (syn-anti), AA (antianti) and AG (antigauche). In consonance with the previous report[9] our calculations predict that three SA isomers (SAA+, SAS and SAA−) stabilized by the intramolecular hydrogen bond between the OH group and the methoxy group oxygen, are the most stable structures with the SAA+ conformer being a global minimum. The stability of two other SA conformers is higher by 1.62 and 2.72 kJ/mol, respectively compared to the SAA+ conformer. The O−H···O hydrogen bond is characterized by the $H_4\cdots O_2$ distance of ca. 2.11 Å, and it is far from linearity with the $O_1H_4O_2$ angle equal to ca. 114°. Both values are very much the same as those predicted for the anisole molecule (2.11 Å, 114.1°) and are within the expected range for this type of interaction. The SA conformers are defined by the $H_4O_1C_7C_2$ dihedral angle value close to 0°,

TABLE 1: Key Torsional Angles (deg), Zero-Point Energy Corrected Relative Energies ΔE_{ZPE}, Relative Gibbs Free Energies ΔG_{298} (kJ/mol) and Abundances *A* (%) at 298 K for All Eugenol Conformers and Three Transition States

minima	$\Phi(H_4O_1C_7C_2)$	$\Phi(C_1O_2C_2C_7)$	$\Phi(C_5C_8C_9C_{10})$	$\Theta(O_1H_4O_2)$	$R(H_4\cdots O_2)$	ΔE	ΔE_{ZPE}	ΔG_{298}	A_{298} (%)
SAA+	0.1	179.6	122.6	114.0	2.111	0.00	0.00	0.0	47.94
SAA−	0.0	179.8	−123.5	113.9	2.117	1.77	1.62	0.38	41.16
SAS	−0.2	179.6	1.8	114.0	2.115	2.78	2.72	3.72	10.70
AAA+	179.8	179.7	122.8			17.87	16.75	16.73	0.06
AAA−	179.9	179.8	−123.5			19.29	18.10	16.49	0.06
AAS	179.8	179.6	1.6			20.47	19.42	20.34	0.01
AGA+	178.0	69.9	122.7			23.51	21.32	19.33	0.02
AGA−	177.9	68.3	−122.7			23.69	21.63	19.97	0.02
AGS	177.7	69.5	0.6			25.47	23.61	23.66	0.00
AGA+′	177.8	68.9	122.8			23.63	21.49	19.98	0.02
AGA−′	177.9	69.9	−123.0			23.69	21.64	20.24	0.01
AGS′	178.2	69.0	−0.5			25.60	23.68	23.44	0.00

TS	$\Phi(H_4O_1C_7C_2)$	$\Phi(C_1O_2C_2C_7)$	$\Phi(C_5C_8C_9C_{10})$	$\Theta(O_1H_4O_2)$	$R(H_4\cdots O_2)$	ΔE	ΔE_{ZPE}	$\nu(cm^{-1})$
$TS_{SAA+SAA-}$	0.00	180.0	178.0	113.9	2.115	9.62	8.32	101i
$TS_{SAA-SAS}$	−0.2	179.3	63.1	114.0	2.113	13.12	12.22	127i
$TS_{SAA+SAS}$	−0.2	180.0	−61.5	113.8	2.119	14.26	13.17	130i

TABLE 2: Values of the Selected Bond Lengths and Valence Angles of the Eugenol Conformers and the Transition States Calculated at the B3LYP/6-311++G(2d,2p) Level

	$R(C_5-C_8)$	$R(C_8-C_9)$	$R(C_9-C_{10})$	$R(C_9-H_{10})$	$\alpha(C_5C_8C_9)$	$\alpha(C_8C_9C_{10})$	$\alpha(H_8C_8H_9)$	$\alpha(C_8C_9H_{10})$	$\alpha(H_{11}C_{10}H_{12})$
SAA+	1.519	1.504	1.328	1.086	113.7	125.1	106.5	115.7	116.9
SAA−	1.519	1.505	1.328	1.086	113.4	125.1	106.5	115.7	116.9
SAS	1.510	1.511	1.327	1.086	116.1	126.8	105.0	114.4	117.1
$TS_{SAA+SAA-}$	1.512	1.519	1.328	1.084	114.0	124.9	105.9	116.0	116.7
$TS_{SAA-SAS}$	1.517	1.520	1.327	1.085	114.6	125.0	106.0	116.4	116.7
$TS_{SAA+SAS}$	1.517	1.521	1.327	1.085	114.5	125.3	106.0	116.2	116.7

	$R(O_1-H_4)$	$R(C_7-O_1)$	$R(C_7-C_2)$	$R(C_2-O_2)$	$R(O_2-C_1)$	$\alpha(H_4O_1C_7)$	$\alpha(O_1C_7C_2)$	$\alpha(C_7C_2O_2)$	$\alpha(C_2O_2C_1)$
SAA+	0.965	1.364	1.405	1.373	1.422	107.8	120.4	114.0	118.3
AAA+	0.961	1.368	1.409	1.361	1.419	109.0	117.3	115.7	118.1
AGA+	0.961	1.371	1.404	1.373	1.432	109.2	118.0	121.6	115.8

and the $C_1O_2C_2C_7$ dihedral angle of ca. 180°. They differ in the values of the $C_5C_8C_9C_{10}$ dihedral angles which are equal to +122.6, −123.5 and +1.8°, for SAA+, SAA− and SAS, respectively, and describe the relative arrangement of the allyl moiety and the aromatic ring.

The second group of the eugenol conformers, denoted as AAA+, AAA- and AAS, is characterized by the $H_4O_1C_7C_2$ angle of ca. 180° and two other dihedral angles of the same values, as in the corresponding SA conformers (SAA+, SAS and SAA−). The AA conformers are 16.75, 18.10 and 19.42 kJ/mol, respectively, higher in energy than the conformational ground state (SAA+).

In the SA and AA conformers both $C_7O_1H_4$ and $C_2O_2C_1$ fragments are coplanar with the benzene ring. In the third group of the eugenol conformers (the AG species) the CH_3 group of the methoxy moiety is tilted above the aromatic ring. Such an arrangement gives rise to six AG conformers: three having both methoxy and allyl groups above the ring plane (AGA+, AGA− and AGS) and three having OCH_3 group above and the allyl moiety below the benzene ring (AGA+′, AGA−′ and AGS′). The AG conformers are calculated to be the least stable structures among all eugenol species. They are predicted to be 21.32−23.68 kJ/mol higher in energy than the SAA+ conformer.

The most significant factor that determines the stability of the eugenol conformers is apparently the intramolecular hydrogen bond that dominates energetically over other interactions. Another factor, however, is also worth mentioning: the importance of interaction involving the $-CH_2CH{=}CH_2$ group and the phenyl ring. Among three SA conformers two (SAA+ and SAA−) have a stretched form with the $-CH_2CH{=}CH_2$ fragment tilting away from the ring and the third of them (SAS) is folded with the terminal CH_2 group hovering over the ring. The latter form was found to be the least stable of the SA species, which is justified by the stronger repulsive interaction between the $CH_2CH{=}CH_2$ group and the aromatic ring in SAS than in SAA+ or SAA−. The same three different arrangements of the $-CH_2CH{=}CH_2$ substituent relative to the ring were found for the AA, AG and AG′ groups of conformers. In all cases the folded structures (AAS, AGS and AGS′) are the least stable forms in the group.

The differences in the geometrical parameters calculated for the various conformers usually do not exceed 0.005 Å for the bond lengths or 3° for the bond angles. Not unexpectedly, larger deviations are noticed in those parts of the eugenol molecule which are expected to be the most sensitive on the conformation adopted, namely the O−H, OCH_3 and $-CH_2CH{=}CH_2$ substituents. In Table 2 the values of the selected structural parameters are compared for the representative conformers and transition states. The highest difference of 0.012 Å is observed for the C_2-O_2 bond and of 7.6° for the $C_7C_2O_2$ bond angle; both parameters describe the methoxy group.

All structural parameters calculated for: SAA+, SAA−, SAS, AAA+ and AGA+ are provided in the Supporting Information in Table S1.

III.2. Population of the Conformers and Conformational Interconversion Barriers. The relative abundance of the studied mixture of conformers was calculated using $\Delta G = -RT \ln K$, where ΔG denotes the difference between Gibbs free energy for given two isomeric forms and K is the equilibrium constant for these species. Because all twelve eugenol conformers have

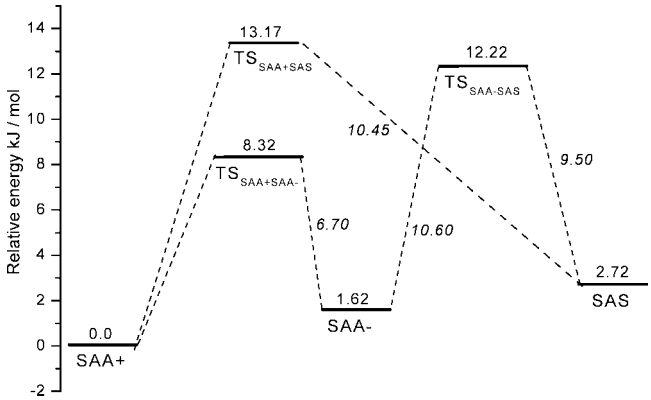

Figure 2. B3LYP/6-311++G(2d,2p) potential energies diagram for the SA isomers. The ZPE corrected energy is in kJ/mol.

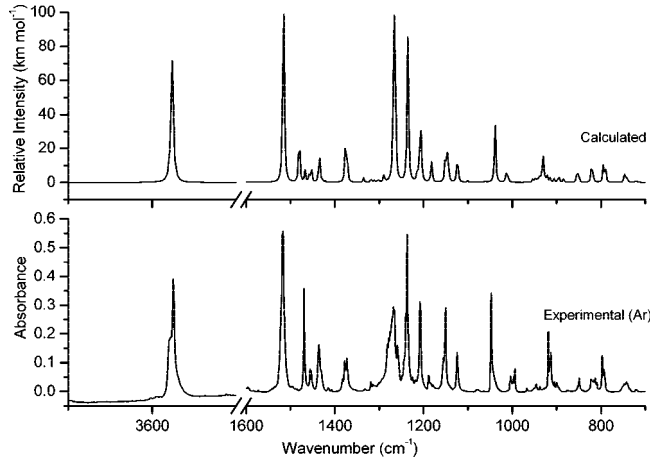

Figure 3. Comparison of the experimental IR spectra of eugenol isolated in Ar matrix at 11 K and the theoretical spectrum obtained by adding the spectra of the SAA+, SAA− and SAS conformers weighted by their respective abundances (47.94, 41.16 and 10.70% for SAA+, SAA− and SAS, respectively). The theoretical spectra were simulated using Lorentzian functions centered at the calculated frequencies scaled by a factor of 0.944 for the 4000−2000 cm^{-1} region and 0.979 for the 2000−500 cm^{-1} region and with the bandwidth-at-half-height equal to 2 cm^{-1}.

the same degeneracy, their abundance in the equilibrium gaseous phase follows the order of the Gibbs free energies which are given in Table 1. The abundance of the most stable SAA+, SAA− and SAS species equals 47.9, 41.2 and 10.7% at 298 K, respectively. The remaining nine structures have a total population of 0.2%. They may be assumed to be of no practical importance and will not be further considered in relation to the experimental spectra.

Knowledge of the barriers to intramolecular rotations in the species of interest is very helpful for the interpretation of the infrared spectra.[13,21] The interconversions of practical interest in the case of eugenol molecule are those between three SA isomers, associated with the changes of the $C_5C_8C_9C_{10}$ dihedral angle. The performed B3LYP/6-311++G(2d,2p) calculations revealed three transition states $TS_{SAA+SAA-}$, $TS_{SAA-SAS}$ and $TS_{SAA+SAS}$, linking three SA conformers on the PES. The structures of these transition states resemble those obtained for the SA species with the exception of the $C_5C_8C_9C_{10}$ dihedral angle values, which are intermediate to those calculated for the SA minima (see Table 1). The relevant potential energy diagram with the associated energy barriers is displayed in Figure 2. The calculated ZPE corrected energy barriers for the SAA− → SAA+ and SAS → SAA+ interconversions are predicted to be of medium height: 6.70 and 10.45 kJ/mol, respectively. On the basis of the available experimental data[19,22,23] one may expect that these barriers are high enough to allow for the simultaneous isolation of all three SA isomers in matrices at the lowest available temperature (11 K). In turn, considering the values of the energy barriers calculated for the SAA− → SAA+ and SAS → SAA+ conversions one may also expect conformational cooling to appear in the matrices studied.

III.3. Interpretation of Matrix Isolated Infrared Spectra. The experimental spectrum of eugenol isolated in an argon matrix deposited at 11K is presented in Figure 3 (lower trace). This figure also shows the spectrum resulting from adding the theoretically predicted IR spectra of three SA conformers scaled by their calculated abundance at room temperature (upper trace). In view of the complexity of the studied system and due to the number of effects which are difficult to simulate such as site-splitting, the agreement between theory and experiment seems to be fairly good.

The interpretation of the experimental results is not straightforward because both the conformational flexibility and the size of the eugenol molecule causes broadness and overlapping of bands in many spectral regions. Inspection of the ν OH region of the experimental spectra allows us to exclude the presence of any of the AAA or AGA conformers. Only one set of the ν OH bands is observed at ca. 3570 cm^{-1} due to the stretching mode of the intramolecularly hydrogen bonded OH group and no trace of the corresponding absorptions due to the free OH group expected at higher wavenumbers, according to the calculations at ca. 3620 cm^{-1}. Thus, to interpret the experimental spectra it was accepted that only three most stable SAA+, SAA− and SAS conformers are present in the studied matrices. The proposed assignment of the IR bands is also based on the analysis of the theoretically predicted spectra and the potential energy distribution (PED) matrices obtained for three SA conformers.

The definition of the internal coordinates used in the performed normal coordinate analysis is given in the Supporting Information in Table S2. The B3LYP/6-311++G(2d,2p) calculated spectra for three most stable eugenol conformers and the corresponding PEDs are gathered in Tables S3−S5. The position of bands observed for the SA conformers in the spectra in solid argon and xenon together with the frequencies predicted by the calculations and their approximate assignment is given in Tables 3–5. In general, the calculated (scaled) spectra fit well the experimental data. The assignment of the absorptions to the individual conformers was facilitated by the intensity dependence of the observed bands, upon changing the temperature of the deposition and on annealing.

Figure 4 shows the infrared spectra in the region of the O−H and C−O (methoxy) stretching modes of eugenol isolated in argon and xenon matrices at different substrate temperature during deposition. The presented experimental spectra are normalized to the same peak intensities of the main (SAA+) form. These spectra are compared with the DFT calculated ones (lower frame) obtained with the frequencies scaled by 0.944 and 0.979 for ν OH and ν CO regions, respectively. It is worth noting that the position of the ν OH frequency observed for the SA conformers at ca. 3575 cm^{-1} (Ar) and ca. 3565 cm^{-1} (Xe) is in good agreement with the result obtained by Castaño and co-workers[9] from the ionization detected IR spectra of eugenol in the molecular supersonic jets. A single, broadband at ca. 3600 cm^{-1} with a full width at half-maximum of ca. 7 cm^{-1} was detected for the SAA+ and SAS conformers.

The theoretically predicted frequencies of the bands due to the O−H and C−O(methoxy) stretching vibrations are very

TABLE 3: Observed and Calculated [B3LYP\6-311++G(2d,2p)] Vibrational Frequencies and IR Intensities of the SAA+ Conformer of the Eugenol Molecule

freq	*I*	freq (scaled)[a]	*I* (scaled)[b]	Ar	Xe	assignment
3788	101	3576	48	3574.7	3563.2	ν OH
3213	15	3034	7	3035.1	3073.0	ν_{as} CH_2 end
3200	1	3021	1	3023.7	n.o.	ν CH ring
3197	9	3018	4	3018.1	n.o.	ν CH ring
3172	10	2994	5	3005.1	2995.2	ν CH ring
3142	19	2966	9	2986.4	n.o.	ν_{as} CH_3
3136	4	2960	2	n.o.	n.o.	ν CH
3128	15	2953	7	n.o.	2953.0	ν_s CH_2 end
3081	28	2908	13	2898.8	n.o.	ν_{as} CH_3
3052	12	2881	6	2870.2	n.o.	ν_{as} CH_2
3023	42	2854	20	2851.3	n.o.	ν_s CH_3
3020	26	2851	12	2833.6	2839.5	ν_s CH_2
1696	18	1661	9	1646.7	1642.9	ν C=C end
1648	17	1614	8	1619.2	1618.5	ν CC ring
1640	10	1606	5	1615.4	1617.9	ν CC ring
1545	194	1513	93	1518.0	1515.0	δ CCH ring + ν CC ring
1511	47	1480	22	1494.8	n.o.	δ_{as} CH_3
1497	9	1466	5	1469.2	1464.8	δ_{as} CH_3
1488	5	1458	2	1455.5	n.o.	δ_s CH_3
1482	18	1452	8	n.o.	n.o.	δ CH_2
1464	24	1434	11	1430.0	1432.6	ν CC ring + δ CCH ring + $\delta_s CH_3$
1457	3	1427	1	n.o.	1427.2	δ CH_2 end
1405	49	1376	24	1373.0	1373.5	δ $OH_{i.p.}$
1345	9	1317	4	1319.1	1313.7	ω CH_2
1329	1	1302	0	n.o.	n.o.	δ CH
1306	1	1279	0	1278.6	1278.3	ω CH_2
1290	220	1264	105	1268.8	1267.7	ν C7−O1 + ν CC ring
1261	155	1235	74	1237.1	1236.0	ν C7−O1 + δ CCC ring
1239	20	1214	9	1219.1	1208.0	r CH_2
1230	52	1205	25	1207.0	1208.6	δ CH_3 + δ $OH_{i.p.}$
1207	14	1182	7	1181.9	1184.8	δ CH_3
1173	1	1149	0	n.o.	n.o.	δ CH_3
1168	54	1144	26	1155.6	1150.0	ν C5−C8 + ν C−OCH_3
1146	18	1123	8	1122.4	1122.7	δ CCH ring
1124	4	1101	2	1078.9	n.o.	r CH_2 end
1060	51	1038	24	1047.5	1049.0	ν C−OCH_3
1033	16	1012	8	1003.6	n.o.	τ CH + τ CH_2end
959	13	939	6	937.9	n.o.	δ CH_2
952	3	933	1	n.o.	n.o.	τ CCH ring
949	16	930	8	920.3	n.o.	τ CH_2 end
941	19	922	9	913.7	914.7	ν C8−C9 + τ CH_2 end
912	11	893	5	899.9	n.o.	r CH_2
873	14	855	7	n.o.	n.o.	τ CCHC ring
835	21	818	10	812.9	814.9	τ CCHC ring
810	29	793	14	793.0	800.2	ν C7−O1 + δ CCC ring
761	21	745	10	740.0	746.2	τ CCCC ring + δ CCC ring
				742.6		
736	3	721	1	720.8	n.o.	τ CCCC ring
				717.5		
657	12	644	6	639.7	n.o.	δ CCC ring + τ CCCC ring

[a] Calculated frequencies scaled applying scaling factor of 0.944 for the 4000−2000 cm^{-1} and 0.979 for the 2000−600 cm^{-1} spectral region. [b] Calculated intensities are scaled by the populations (see Table 1).

TABLE 4: Observed and Calculated[a] [B3LYP\6-311++G(2d,2p)] Vibrational Frequencies and IR Intensities of the SAA− Conformer of the Eugenol Molecule

freq	freq	freq (scaled)[a]	*I* (scaled)[b]	Ar	Xe	assignment
3789	106	3577	44	3578.3	3565.2	ν OH
3215	15	3035	6	3031.0	3077.0	ν_{as} CH_2 end
3197	2	3018	1	n.o.	n.o.	ν CH ring
3194	10	3015	4	3015.8	n.o.	ν CH ring
3178	6	3000	2	3007.0	n.o.	ν CH ring
3141	19	2965	8	2970.0	n.o.	ν_{as} CH_3
3137	4	2961	2	n.o.	n.o.	ν CH
3130	16	2955	7	2948.0	n.o.	ν CH + ν_s CH_2end
3078	30	2906	12	2926.0	n.o.	ν_{as} CH_3
3054	13	2883	5	2898.2	n.o.	ν_{as} CH_2
3021	61	2852	25	2873.0	2841.8	ν_s CH_3
3020	11	2851	4	2851.9	n.o.	ν_s CH_2
1696	17	1661	7	1644.9	1640.1	ν C=C end
1646	23	1612	9	1623.7	1615.5	ν CC ring
1640	20	1606	8	1608.5	1610.9	ν CC ring
1547	197	1515	81	1516.9	1518.9	δ CCH ring + ν CC ring
1510	45	1479	19	n.o.	n.o.	δ_{as} CH_3
1497	9	1466	4	n.o.	n.o.	δ_{as} CH_3
1487	9	1457	4	1455.8	n.o.	δ_s CH_3
1485	3	1455	1	1453.6	n.o.	δ CH_2
1464	24	1434	10	1436.2	n.o.	δ_s CH_3 + ν CC ring
1458	1	1428	0	1430.4	1428.3	δ CH_2 end
1400	55	1371	23	1377.9	1370.2	$\delta OH_{i.p.}$
1337	4	1310	2	1314.0		ω CH_2
1328	2	1301	1	n.o.	1296.7	δ CH
1316	17	1289	7	1281.7	1276.1	ω CH_2
1293	214	1267	88	1259.3	1256.4	ν C7−O1 + ν CC ring
1260	142	1234	59	1234.1	1231.0	ν C7−O1 + δ CCC ring
1235	29	1210	12	1208.0	1204.7	r CH_2
1230	47	1205	19	1208.3	1200.2	δ CH_3 + δ $OH_{i.p.}$
1205	16	1180	7	1188.5	1188.6	δ CH_3
1173	5	1149	2	n.o.	n.o.	δ CH_3
1170	52	1146	21	1150.3	1151.5	ν C5−C8 + δ CCH ring
1148	31	1125	13	1124.5	n.o.	δ CCH ring
1122	1	1099	0	1078.9	n.o.	r CH_2 end
1060	59	1038	24	1048.0	1046.3	ν C−OCH_3
1030	18	1009	7	n.o.	n.o.	τ CH + τ CH_2end
966	13	946	5	945.3	n.o.	ν C8−C9
959	2	939	1	n.o.	n.o.	τ CCHC ring
948	44	930	18	918.9	913.7	τ CH_2 end
924	8	905	3	904.9	n.o.	r CH_2 end
916	6	897	2	901.8	n.o.	δ CH_2
868	16	850	6	847.3	n.o.	τ CCHC ring
839	20	822	8	822.4	818.1	τ CCHC ring
810	22	793	9	792.1	800.2	ν C7−O1 + δ CCC ring
				790.7		
763	11	747	5	750.8	746.2	τ CCCC ring + δ CCC ring
				747.8		
736	1	721	0	n.o.	n.o.	τ CCCC ring
662	11	647	4	647.6	n.o.	δ CCC ring + τ CCCC ring

[a] Calculated frequencies scaled applying scaling factor of 0.944 for the 4000−2000 cm^{-1} and 0.979 for 2000−600 cm^{-1} spectral region, [b] Calculated intensities are scaled by the populations (see Table 1).

much the same in three SA conformers (see Tables 3–5). However, the obtained experimental spectra allowed these absorptions to be nicely distinguished. In the spectra of the argon matrices the main maximum in the region of the ν OH mode is

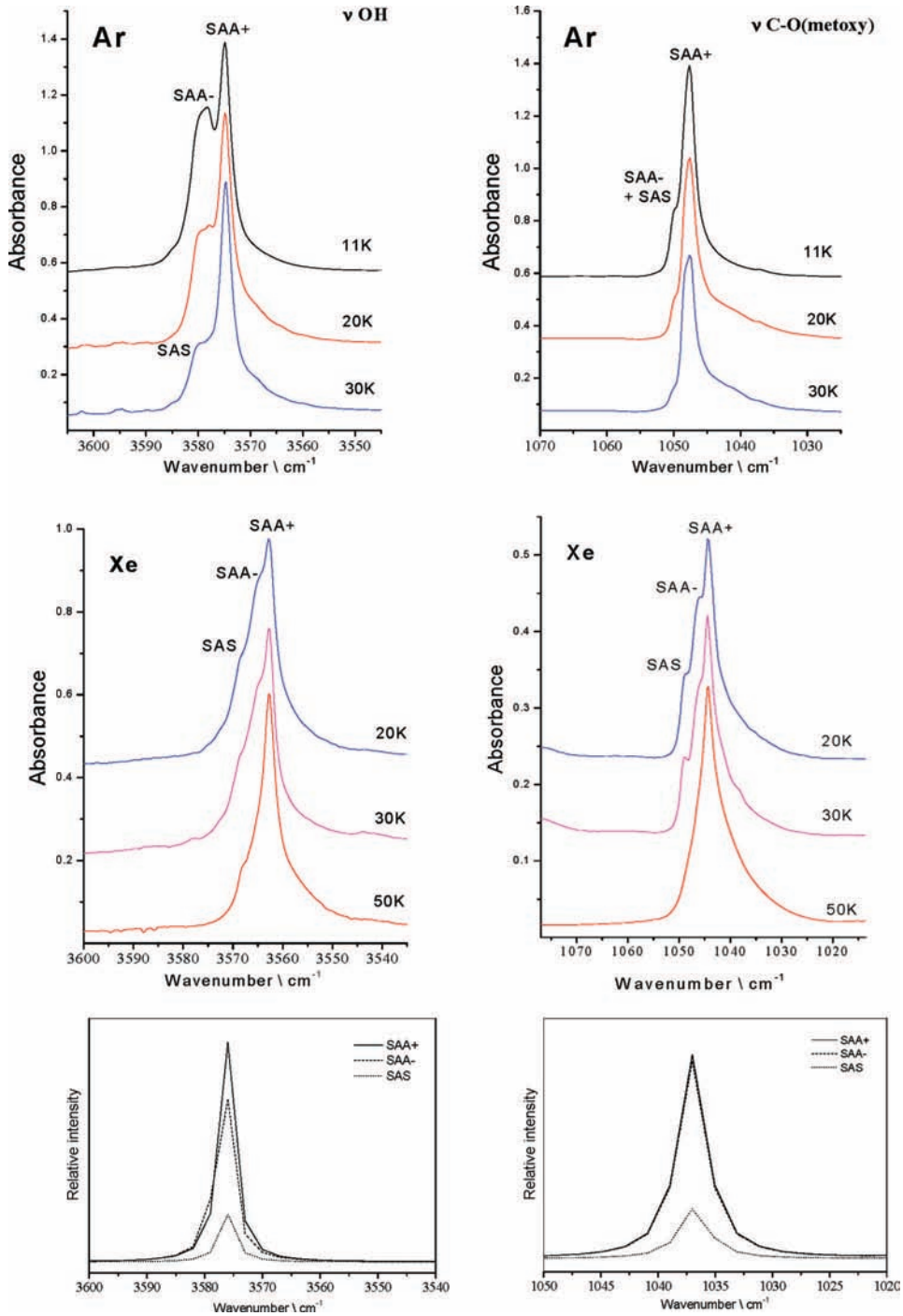

Figure 4. ν OH and ν CO(methoxy) regions of the spectra of the eugenol molecule isolated in argon and xenon matrices at different deposition temperature. The lower frames show the B3LYP/6-311++G(2d,2p)-predicted spectra of SAA+, SAA− and SAS.

situated at 3574.7 cm^{-1} (see Figure 4) and two shoulders are observed at 3578.3 and 3580.6 cm^{-1}. In xenon matrices the corresponding bands are present at 3563.2, 3565.2 and 3568.5 cm^{-1}. In the ν C−O region the maximum absorption is recorded at 1047.5 (Ar) and 1049.0 cm^{-1} (Xe) with the accompanying bands appearing at 1048.0 and 1049.9 cm^{-1} (Ar) and at 1046.3 and 1049.0 cm^{-1} (Xe). The theoretically predicted room temperature abundance of the SAA+, SAA− and SAS conformers equals 47.9, 41.2 and 10.7%, which allows us to assign the most intense band at 3574.7 (Ar) and 3563.2 cm^{-1} (Xe) to the SAA+ conformer. The less populated form (SAA−) is characterized by the absorption at 3578.3 (Ar) and 3565.2 cm^{-1}(Xe), whereas the least intense bands at 3580.6 (Ar) and 3568.5 cm^{-1} (Xe) are assigned to the SAS conformer.

Figure 5 shows three other selected regions of the spectra obtained in xenon matrices at various substrate temperatures during deposition. Similar three-component absorptions due to the SAA+, SAA− and SAS conformers are observed in these regions as well. According to the theoretical predictions a number of other frequencies, especially due to the modes of the allyl moiety and the aromatic ring is expected to differ by 5−10 cm^{-1} for the SAA+, SAA− and SAS conformers. However, they are characterized by very low intensities what prevents observation of their splitting (see Tables 3−5).

The theoretically predicted energy barriers of 6.70 and 10.45 kJ/mol for SAA− → SAA+ and SAS → SAA+ interconversions, respectively, belong to the medium height energy barriers. According to the relationship proposed by Barnes,[21] both SAA−

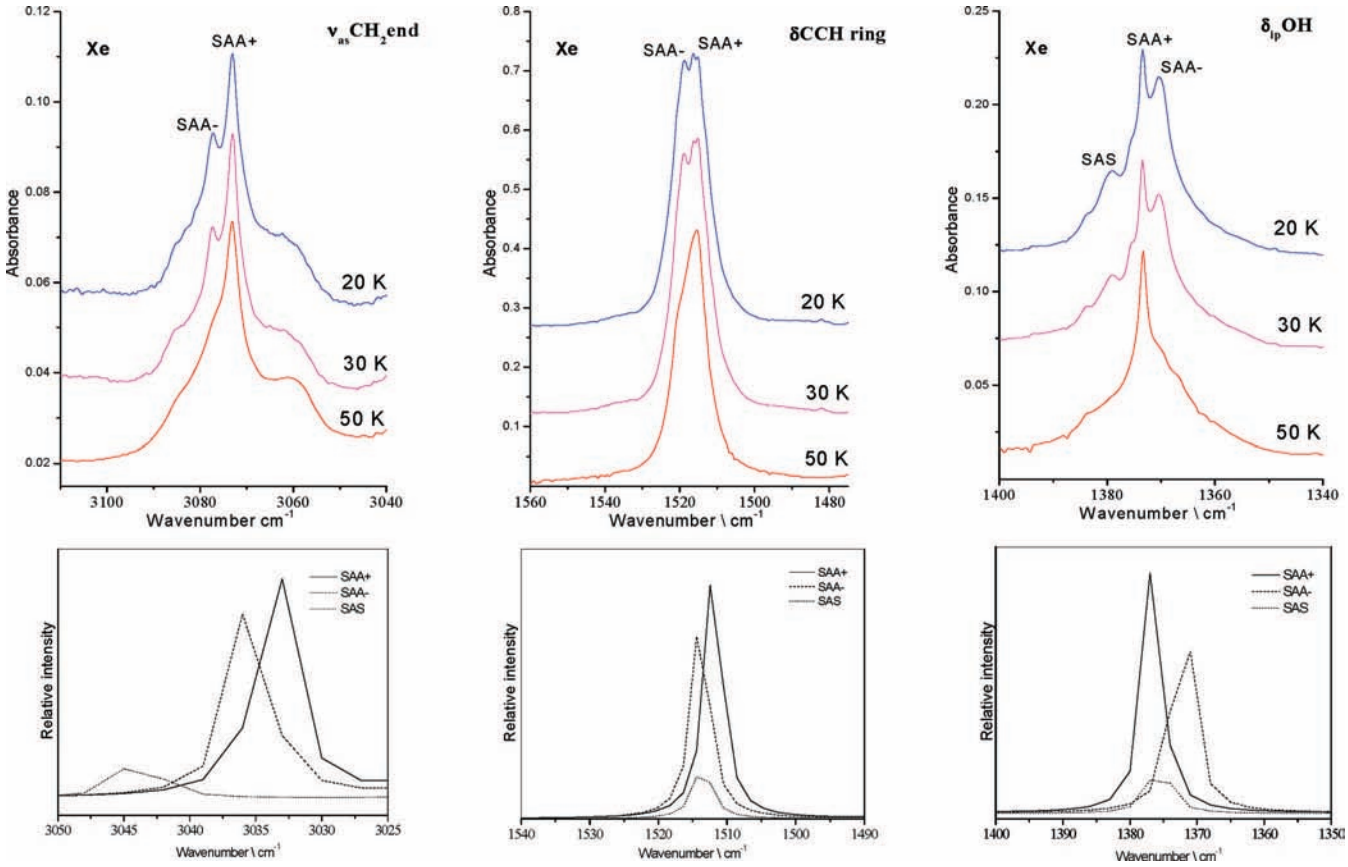

Figure 5. ν_{as} CH_2, δ CCH ring, δ_{ip} OH regions of the spectra of eugenol molecule isolated xenon matrices at different deposition temperature. The lower frames show the B3LYP/6-311++G(2d,2p)-predicted spectra of SAA+, SAA− and SAS conformers.

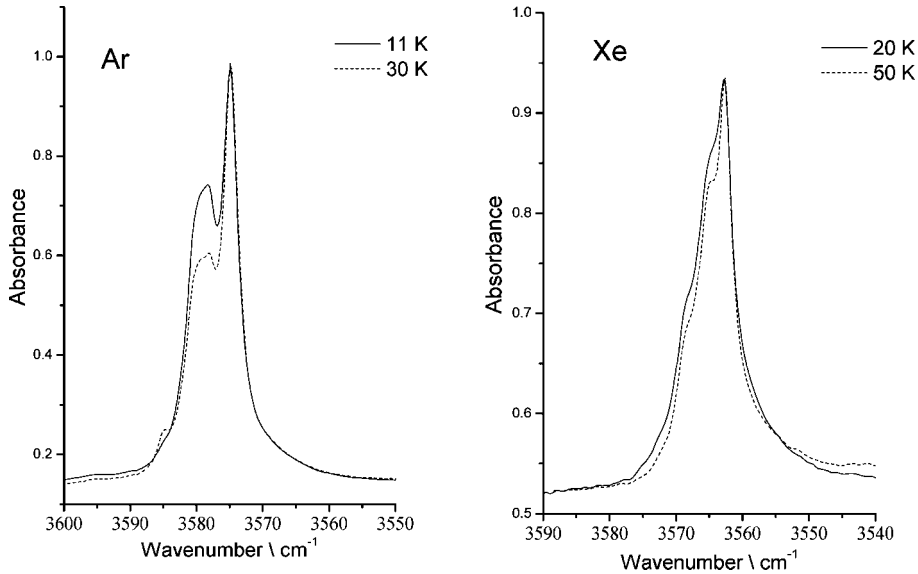

Figure 6. ν OH region in the spectra of the eugenol isolated in Ar and Xe matrices registered directly after sample deposition (solid line), and after annealing (dashed line) up to 30 K (Ar) or 50 K (Xe).

→ SAA+ and SAS → SAA+ processes may occur under our experimental conditions in Ar and Xe matrices. As can be seen from Figures 4 and 5, increasing the deposition temperature results in the decrease of intensity of the bands assigned to the SAA− and SAS conformers and, simultaneously, the increase of the SAA+ absorptions is observed. Thus, the conversion of the less stable SAA− and SAS conformers into SAA+ is detected in the studied spectra showing that the conformational cooling process appears during deposition of the matrices. At lower substrate temperatures all three conformers are present, whereas at 50 K in xenon the conformational cooling process seems to be completed and bands due to the SAA− and SAS species are practically not observed in the spectra.

It is generally accepted that xenon is a better matrix-gas to induce conformational cooling than argon.[13,24,25] It means that in the spectra of xenon matrices one should expect higher SAA+/SAA− and SAA+/SAS population ratios as compared with the argon experiment performed at the same temperature. The closer inspection of Figure 4 reveals that our experimental data are not consistent with this assumption. In both ν OH and

TABLE 5: Observed and Calculated[a] [B3LYP\6-311++G(2d,2p)] Vibrational Frequencies and IR Intensities of the SAS Conformer of the Eugenol Molecule

freq	I	freq (scaled)[a]	I (scaled)[b]	Ar	Xe	sssignment
3788	101	3576	11	3580.6	3568.5	ν OH
3224	14	3043	1	3106.5	n.o.	ν_{as} CH_2 end
3197	1	3018	0	n.o.	n.o.	ν CH ring
3194	10	3015	1	n.o.	n.o.	ν CH ring
3173	9	2995	1	n.o.	n.o.	ν CH ring
3145	7	2969	1	n.o.	n.o.	ν_s CH_2 end
3142	18	2966	2	n.o.	n.o.	ν_{as} CH_3
3124	31	2949	3	n.o.	n.o.	ν CH
3080	28	2908	3	2907.1	n.o.	ν_{as} CH_3
3032	13	2862	1	2873.0	n.o.	ν_{as} CH_2
3022	45	2853	5	2852.5	n.o.	ν_s CH_3
3010	29	2841	3	2838.0	n.o.	ν_s CH_2
1698	19	1663	2	1653.0	n.o.	ν C=C end
1648	19	1614	2	1620.8	n.o.	ν CC ring
1642	16	1608	2	1608.2	n.o.	ν CC ring
1547	180	1515	19	1521.1	1516.8	δ CCH ring + ν CC ring
1511	45	1480	5	1498.5	n.o.	δ_{as} CH_3
1497	9	1466	1	1464.8	n.o.	δ_{as} CH_3
1487	4	1457	0	n.o.	n.o.	δ_s CH_3
1482	12	1452	1	n.o.	n.o.	δ CH_2
1465	28	1435	3	n.o.	n.o.	δ_s CH_3 + ν CC ring
1451	3	1421	0	n.o.	n.o.	δ CH_2 end
1404	56	1375	6	1375.7	1379.3	δ $OH_{i.p.}$ + ν CC ring
1362	11	1334	1	n.o.	n.o.	ω CH_2
1331	2	1304	0	n.o.	n.o.	δ CH
1328	1	1301	0	n.o.	n.o.	ω CH_2
1292	209	1266	22	1257.0	1276.0	ν C7−O1 + ν CC ring
1262	134	1236	14	1244.2	1228.0	ν C7−O1 + δ CCC ring
1232	70	1207	7	1207.8	1211.1	δ $OH_{i.p}$
1214	1	1189	0	n.o.	n.o.	r CH_2
1206	27	1181	3	1190.3	n.o.	δ CH_3
1175	59	1151	6	1159	n.o.	ν C1−O2
1174	1	1150	0	n.o.	n.o.	δ CH_3
1145	21	1122	2	1117.4	n.o.	ν C5−C8 + δ CCH ring
1082	3	1060	0	1058.9	n.o.	r CH_2 end
1060	56	1038	6	1049.9	1049.0	ν C−OCH_3
1035	11	1014	1	1010.9	n.o.	τ CH + τ CH_2end
973	9	953	1	n.o.	n.o.	δ CH_2
954	0	934	0	n.o.	n.o.	τ CCHC ring
953	23	933	2	929.9	n.o.	τ CH_2 end
933	10	914	1	911.8	n.o.	r CH_2
902	10	884	1	n.o.	n.o.	ν C8−C9
870	12	852	1	n.o.	n..o.	τ CCHC ring
837	18	820	2	n.o.	n.o.	τ CCHC ring
806	30	790	3	n.o.	n.o.	ν C7−O1 + ν C7−O2
755	9	740	1	734.3	739.9	τ CCCC ring
730	3	715	0	n.o.	n.o.	τ CCCC ring
659	11	646	1	643.0	n.o.	τ CCCC ring

[a] Calculated frequencies scaled applying scaling factor of 0.944 for the 4000−2000 cm^{-1} and 0.979 for the 2000−600 cm^{-1} spectral region. [b] Calculated intensities are scaled by the populations (see Table 1).

ν CO regions, the bands assigned to the less stable SAA− and SAS conformers are slightly more intense in xenon than in argon matrices at a given temperature as compared with the corresponding SAA+ absorptions. A similar pattern is observed in other spectral regions of the studied matrices. These observations can be explained as follows. The performed B3LYP/6-311++G(2d,2p) calculations have revealed that two less stable SAA− and SAS conformers are more polar molecules than is the SAA+ conformer. The predicted dipole moments are equal to 2.51, 2.81 and 2.75 D for SAA+, SAA− and SAS, respectively. Thus the observed higher abundance of the less stable conformers in xenon matrix as compared with solid argon may be explained in terms of the stabilization increase of more polar molecules in more polarizable Xe medium.[13] This is in agreement with previously reported observations;[24] the relative population of the ASC (μ = 1.40 D) and GSC (μ = 1.99 D) conformers of *N*,*N*-dimethylglycine methyl ester in argon and xenon matrices under the same experimental conditions was found to differ noticeable, with the less stable but more polar GSC species being more abundant in xenon than in argon.

The bands due to the SAA+, SAA− and SAS species overlap practically in all spectral regions. This precludes us from even rough estimating the experimental abundances based on the ratio of the integral band intensities of the considered conformers. However, an estimation was made for the integral intensities of the overall absorptions for the ν OH and ν CO modes in the spectra of both Ar and Xe matrices recorded at different substrate temperatures during deposition to check for possible aggregation effects. The results of this estimation clearly indicate that the sum integral intensities of the particular absorption remains constant upon temperature changes confirming that the described interconversions occur at the monomer level before aggregates are formed.

As could be anticipated, the results of the annealing of the matrices after deposition are similar to those discussed above, obtained at the varying substrate temperature. The annealing of the argon matrix at 30 K and the xenon matrix at 50 K brings an increase of the intensity of the bands assigned to SAA+, with simultaneous decrease of the SAA− and SAS absorptions. A similar pattern, shown in Figure 6 for the ν OH region, is observed for other modes in both matrices. It is also worth noting that after annealing at 35 K (not shown) of argon matrices aggregation occurs as indicated by appearance of new bands in a number of spectral regions. This process was practically not observed in the xenon matrices up to 60 K, most probably because of slightly different experimental conditions used (larger matrix-gas flux) resulting in lower concentration of eugenol in Xe than in Ar.

The results described above unequivocally prove that all three SA conformers are present in the studied matrices and that the interconversion between the individual conformers SAA+, SAA− and SAS takes place. The presence of two of SA conformers of eugenol have been already reported by Castaño et al.[9] who studied this molecule in supersonic expansion using a number of complementary laser spectroscopic techniques. Two sets of bands in the REMPI spectrum have been detected that have originated from two SA conformers (here denoted as SAA+ and SAS); however, the second as to the energy, SAA− conformer, identified in our matrices, was not present in the supersonic jets. As explained by Castaño et al., the energy barrier between SAA+ and SAA− is low enough to allow a population exchange. In contrast, the energy barrier between SAA+ and SAS is high enough to preclude any population migration during the expansion cooling.[9] In turn, the observation of all three most stable conformers of eugenol in matrices is justified by apparently different conditions of their isolation without adiabatic cooling typical for the supersonic expansion.

IV. Conclusions

The systematic search on the PES at the B3LYP/6-311++G(2d,2p) level of eugenol revealed the presence of twelve different conformers. All optimized structures can be divided into three groups differing in the relative orientation of the OH and OCH_3 moieties: SA (syn-anti), AA (antianti) and AG (antigauche). The SA (SAA+, SAA− and SAS) conformers are stabilized by the intramolecular hydrogen bond and are far more stable and abundant (99.8%) than the remaining AA and AG species with the total population of 0.2%. The lowest-energy SA conformers of eugenol differ in the arrangement of the allyl moiety with respect to the aromatic ring.

Matrix isolation FTIR spectroscopy allowed, for the first time, unequivocal observation and spectral characterization of three SA conformers of the eugenol molecule. The assignment of the experimental spectra was carried out on the basis of comparison with the theoretical spectra and temperature variation data (change of the substrate temperature, annealing experiments). In consonance with the theoretical predictions, only SA conformers are present in low temperature matrices and SAA+, which represents the global minimum is the dominant species trapped in both argon and xenon matrices.

The conformational behavior of the SA conformers of eugenol in argon and xenon matrices indicates that conformational cooling (upon increasing the substrate temperature during deposition) takes place in the studied matrices and the conversion of the less stable SAA− and SAS species into SAA+ occurs at the monomer level before the formation of aggregates. This observation appeared to be consistent with the theoretically predicted energy barriers of 6.70 and 10.45 kJ/mol for the SAA− → SAA+ and SAS → SAA+ interconversions, which are low enough to be surpassed during deposition at higher temperatures.

Supporting Information Available: Calculated geometric parameters for the selected conformers and transition states of eugenol (Table S1), definition of internal coordinates (Table S2), normal coordinate analysis results for SAA+, SAA− SAS (Tables S3−S5). This material is available free of charge via the Internet at http://pubs.acs.org.

Acknowledgment. A grant of computer time from the Wrocław Center for Networking and Supercomputing is gratefully acknowledged.

References and Notes

(1) Fujisawa, S.; Atsumi, T.; Kadoma, Y.; Ishihara, M.; Ito, S.; Yokoe, I. *Anticancer Res.* **2004**, *24*, 3019.

(2) Tampieri, M. P.; Galuppi, R.; Macchioni, F.; Carelle, M. S.; Falcioni, L.; Cioni, P. L.; Morelli, I. *Mycopathologia* **2005**, *159*, 339.

(3) Rojo, L.; Vazquez, B.; Parra, J.; Bravo, A. L.; Deb, S.; Roman, J. S. *Biomacromolecules* **2006**, *7*, 2751.

(4) Sato, K.; Krist, S.; Buchbauer, G. *Biol. Pharm. Bull.* **2006**, *29*, 2292.

(5) Chaieb, K.; Hajlaoui, H.; Zmantar, T.; Ben Kahla-Nakbi, A.; Rouabhia, M.; Mahdouani, K.; Bakhrouf, A. *Phytother. Res.* **2007**, *21*, 501.

(6) Nangia-Makker, P.; Tail, L.; Shekhar, M. P. V.; Palomino, E.; Hogan, V.; Piechocki, M. P.; Funasaka, T.; Raz, A. *Int. J. Cancer* **2007**, *121*, 884.

(7) Laekeman, G. M.; Van Hoof, L.; Haemers, A.; Vanden Berghe, D.; Herman, A. G.; Vlietinck, A. *J. Phytother. Res.* **1990**, *4*, 90.

(8) He, M.; Du, M. Q.; Fan, M. W.; Bian, Z. A. *Mycopathologia* **2007**, *163*, 137.

(9) Longarte, A.; Unamuno, I.; Fernández, J. A.; Castaño, F.; Redondo, C. *J. Chem. Phys.* **2004**, *121*, 209.

(10) Longarte, A.; Redondo, C.; Fernández, J. A.; Castaño, F. *J. Chem. Phys.* **2005**, *122*, 164304.

(11) Kaczor, A.; Reva, I. D.; Proniewicz, L. M.; Fausto, R. *J. Phys. Chem. A* **2007**, *111*, 2957.

(12) Haas, Y.; Samuni, U. *Prog. React. Kinet.* **1998**, *23*, 211.

(13) Reva, I. D.; Stepanian, S. G.; Adamowicz, L.; Fausto, R. *Chem. Phys. Lett.* **2003**, *374*, 631.

(14) Stepanian, S. G.; Reva, I. D.; Radchenko, E. D.; Rosado, M. T. S.; Duarte, M. L. T. S.; Fausto, R.; Adamowicz, L. *J. Phys. Chem. A* **1998**, *102*, 1041.

(15) Kudoh, S.; Takayanagi, M.; Nakata, M. *Chem. Phys. Lett.* **1998**, *296*, 329.

(16) Reva, I. D.; Lopes Jesus, A. J.; Rosado, M. T. S.; Fausto, R.; Eusébio, M. E.; Redinha, J. S. *Phys. Chem. Chem. Phys.* **2006**, *8*, 5339.

(17) Reva, I. D.; Jarmelo, S.; Lapinski, L.; Fausto, R. *Chem. Phys. Lett.* **2004**, *389*, 68.

(18) Reva, I.; Simão, A.; Fausto, R. *Chem. Phys. Lett.* **2005**, *406*, 126.

(19) Borba, A.; Gomez-Zavaglia, A.; Fausto, R. *J. Mol. Struct.* **2006**, *794*, 196.

(20) M. J. Frisch, G. W. Trucks, H. B. Schlegel, G. E. Scuseria, M. A. Robb, J. R. Cheeseman, J. A. Montgomery, Jr., T. Vreven, K. N. Kudin, J. C. Burant, J. M. Millam, S. S. Iyengar, J. Tomasi, V. Barone, B. Mennucci, M. Cossi, G. Scalmani, N. Rega, G. A. Petersson, H. Nakatsuji, M. Hada, M. Ehara, K. Toyota, R. Fukuda, J. Hasegawa, M. Ishida, T. Nakajima, Y. Honda, O. Kitao, H. Nakai, M. Klene, X. Li, J. E. Knox, H. P. Hratchian, J. B. Cross, V. Bakken, C. Adamo, J. Jaramillo, R. Gomperts, R. E. Stratmann, O. Yazyev, A. J. Austin, R. Cammi, C. Pomelli, J. W. Ochterski, P. Y. Ayala, K. Morokuma, G. A. Voth, P. Salvador, J. J. Dannenberg, V. G. Zakrzewski, S. Dapprich, A. D. Daniels, M. C. Strain, O. Farkas, D. K. Malick, A. D. Rabuck, K. Raghavachari, J. B. Foresman, J. V. Ortiz, Q. Cui, A. G. Baboul, S. Clifford, J. Cioslowski, B. B. Stefanov, G. Liu, A. Liashenko, P. Piskorz, I. Komaromi, R. L. Martin, D. J. Fox, T. Keith, M. A. Al-Laham, C. Y. Peng, A. Nanayakkara, M. Challacombe, P. M. W. Gill, B. Johnson, W. Chen, M. W. Wong, C. Gonzalez, and J. A. Pople, *Gaussian 03*, Revision C.02; Gaussian, Inc.: Wallingford, CT, 2004.

(21) Barnes, A. J. *J. Mol. Struct.* **1984**, *113*, 161.

(22) Borba, A.; Gomez-Zavaglia, A.; Lapinski, L.; Fausto, R. *Phys. Chem. Chem. Phys.* **2004**, *6*, 2101.

(23) Borba, A.; Gomez-Zavaglia, A.; Simões, P. N. N. L.; Fausto, R. *J. Phys. Chem. A* **2005**, *109*, 3578.

(24) Gómez-Zavaglia, A.; Fausto, R. *Phys. Chem. Chem. Phys.* **2003**, *5*, 52.

(25) Kaczor, A.; Pinho e Melo, T. M. V. D.; Soares, M. I. L.; Fausto, R. *J. Phys. Chem. A* **2006**, *110*, 6531.

JP801430D